

UC Irvine

UC Irvine Previously Published Works

Title

Quantitative Evaluation of Adult Subglottic Stenosis Using Intraoperative Long-range Optical Coherence Tomography

Permalink

<https://escholarship.org/uc/item/9js6z3xq>

Journal

Annals of Otology Rhinology & Laryngology, 125(10)

ISSN

0003-4894

Authors

Sharma, Giriraj K
Loy, Anthony Chin
Su, Erica
et al.

Publication Date

2016-10-01

DOI


10.1177/0003489416655353

Copyright Information

This work is made available under the terms of a Creative Commons Attribution License, available at <https://creativecommons.org/licenses/by/4.0/>

Peer reviewed

Quantitative Evaluation of Adult Subglottic Stenosis Using Intraoperative Long-range Optical Coherence Tomography

Annals of Otolaryngology, Rhinology & Laryngology
2016, Vol. 125(10) 815–822
© The Author(s) 2016
Reprints and permissions:
sagepub.com/journalsPermissions.nav
DOI: 10.1177/0003489416655353
aor.sagepub.com


Giriraj K. Sharma, MD, MS¹, Anthony Chin Loy, MD¹, Erica Su, BS², Joe Jing, MS^{2,3}, Zhongping Chen, PhD^{2,3}, Brian J-F. Wong, MD, PhD¹, and Sunil Verma, MD^{1,4}

Abstract

Objectives: To determine the feasibility of long-range optical coherence tomography (LR-OCT) as a tool to intraoperatively image and measure the subglottis and trachea during suspension microlaryngoscopy before and after endoscopic treatment of subglottic stenosis (SGS).

Methods: Long-range optical coherence tomography of the adult subglottis and trachea was performed during suspension microlaryngoscopy before and after endoscopic treatment for SGS. The anteroposterior and transverse diameters, cross-sectional area (CSA), distance from the vocal cords, and length of the SGS were measured using a MATLAB software. Pre-intervention and postintervention airway dimensions were compared. Three-dimensional volumetric airway reconstructions were generated using medical image processing software (MIMICS).

Results: Intraoperative LR-OCT imaging was performed in 3 patients undergoing endoscopic management of SGS. Statistically significant differences in mean anteroposterior diameter ($P < .01$), transverse diameter ($P < .001$), and CSA ($P < .001$) were noted between pre-intervention and postintervention data. Three-dimensional airway models were viewed in cross-sectional format and via virtual “fly through” bronchoscopy.

Conclusions: This is the first report of intraoperative LR-OCT of the subglottic and tracheal airway before and after surgical management of SGS in humans. Long-range optical coherence tomography offers a practical means to measure the dimensions of SGS and acquire objective data on the response to endoscopic treatment of SGS.

Keywords

subglottic stenosis, optical coherence tomography, airway measurement, direct laryngoscopy, suspension microlaryngoscopy

Introduction

Subglottic stenosis (SGS) occurs as a consequence of trauma, prolonged endotracheal intubation, infectious and chronic inflammatory diseases,^{1,2} or for idiopathic³ reasons and remains a therapeutic challenge for otolaryngologists. Evaluation of the airway and characterization of stenosis is a critical aspect of SGS management. Serial airway evaluation of patients with SGS is also important to gauge treatment efficacy and the rate of disease recurrence. At present, however, there are limited options to practically and accurately measure the cross-sectional dimensions of SGS and quantify the efficacy of treatment.

The most widely used objective measure of SGS in clinical practice is the Cotton-Myer grading system.⁴ This SGS classification scheme requires interchanging of endotracheal tubes to yield a crude estimate of the percentage of airway stenosis and does not accurately

measure nonconcentric stenosis. Diagnostic imaging options for evaluation and measurement of SGS include computed tomography (CT) and magnetic resonance (MR) imaging. Thin-cut CT may be used to measure airway dimensions in the transverse and cranio-caudal

¹Department of Otolaryngology-Head and Neck Surgery, University of California, Irvine, California, USA

²Beckman Laser Institute, University of California, Irvine, California, USA

³Department of Biomedical Engineering, University of California, Irvine, California, USA

⁴University Voice and Swallowing Center, University of California, Irvine, California, USA

Corresponding Author:

Sunil P. Verma, MD, University Voice and Swallowing Center, Department of Otolaryngology-Head & Neck Surgery, University of California, Irvine, 62 Corporate Park #115, Irvine, CA 92606, USA.
Email: verma@uci.edu

dimensions to within 1 mm accuracy.⁵ However, CT is associated with ionizing radiation exposure.⁶ Magnetic resonance also lacks adequate spatial resolution for precise millimeter-scale anatomic measurements⁷ and, along with CT, is associated with increased cost and requires a separate visit for the patient. In 2015, the “measuring stick” was described as a practical solution for measuring SGS diameter and length during suspension microlaryngoscopy.⁸ This instrument, easily constructed from Kirschner (K) wires, allows for accurate measurement of SGS diameter and length but does not permit data capture for offline image analysis or 3-dimensional (3-D) digital reconstruction of the airway. Options for endoscopic evaluation of the subglottis and trachea include office-based transnasal tracheoscopy under topical anesthesia,⁹ flexible bronchoscopy, and direct laryngoscopy and rigid bronchoscopy (DLB). During endoscopy, the airway diameter can be estimated by comparing the size of the endoscope tip to the lumen of the airway. However, this measure is imprecise due to fish-eye optical distortion associated with distal-chip endoscopes.¹⁰

Optical coherence tomography (OCT) is a minimally invasive diagnostic imaging modality that is widely used in ophthalmologic^{11,12} and intravascular^{13,14} imaging and is currently the focus of intensive translational research in upper airway imaging.¹⁵⁻¹⁹ Optical coherence tomography provides high-resolution (~10 micron), cross-sectional imaging of biological tissue with up to 1 to 2 mm depth.²⁰ Long-range OCT (LR-OCT) is a derivative of OCT that is optimized for intraluminal topographical mapping of large, hollow organs such as the airway.¹⁵⁻¹⁹ Previous studies have utilized LR-OCT to analyze upper airway size and shape in patients with obstructive airway disease.^{21,22} The accuracy of OCT in measuring the airway has been previously validated by studies comparing OCT with CT of *in vivo* airways¹⁷ or with caliper measurements of airway phantoms.²³

Given the efficacy and accuracy of quantitative LR-OCT of the airway, this technology was applied to the measurement of SGS. The objective of this study was to perform quantitative LR-OCT of the adult upper airway during suspension microlaryngoscopy before and after endoscopic management of SGS. This is the first report of intraoperative OCT of the adult airway with objective comparison of pre-intervention and postintervention luminal patency.

Methods

Study Design

Approval for this study was obtained from the human subjects Institutional Review Board at the University of California, Irvine (HS No. 2003-3025). A prospective clinical trial was conducted to evaluate LR-OCT of the upper

airway in adults undergoing endoscopic treatment of SGS. Subjects included adult patients with SGS undergoing first-time treatment for SGS. All patients provided written informed consent for participation in the study.

Long-range Optical Coherence Tomography System

A swept-source Fourier domain LR-OCT system was constructed (Figure 1A). Technical parameters have been previously described,²⁴ and only a brief summary is provided in the following. The LR-OCT system utilized a near-infrared swept-source laser (central wavelength 1310 nm; Axsun Technologies; Billerica, Massachusetts, USA) and achieved an axial resolution of ~10 μm with a full axial range of up to 10 mm. The output light was split by a 90:10 coupler into a sample arm (airway tissue) and a reference arm (mirror), respectively. An acousto-optic modulator was used in the reference arm to generate a carrier frequency of 100 MHz, enabling “long range” axial imaging of lumen diameters up to 20 mm.

Flexible, side-view probes (outer diameter/OD 1.2 mm) were constructed using an optical fiber encased in a torque coil coupled with a Gradient Index Rod (GRIN) lens (Figure 1B). The probe was proximally connected to an external rotational motor that allowed for high-speed rotation (25 Hz) and retraction of the probe along the longitudinal axis of the airway. Images were acquired in a retrograde, helical format, and consecutive 360° frames were separated by 500 μm .

Intraoperative LR-OCT

Long-range optical coherence tomography imaging of the subglottic and tracheal airway was performed in the operating room under suspension microlaryngoscopy. Patients were anesthetized and placed in suspension for laryngeal microsurgery, and jet ventilation was used as needed. Initially, the airway was visualized using a zero-degree rigid endoscope. The LR-OCT probes were encased in a transparent fluorinated ethylene propylene (FEP) sheath (2.08 mm OD; Zeus Inc, Orangeburg, South Carolina, USA). The surgeon (S.V.) introduced the probe through the laryngoscope and positioned the distal tip of the probe in the center of the airway lumen, approximately 5 mm distal to the segment of stenosis. Next, the probe was mechanically rotated and retracted within the stationary sheath to produce a volumetric data set starting in the healthy, proximal trachea and terminating at the glottis. The time to perform imaging was noted, and OCT data were recorded to a PC hard drive in real-time. The SGS was then managed with a combination of carbon-dioxide laser lysis of scar and balloon dilatation of the airway. The LR-OCT imaging was repeated post intervention.

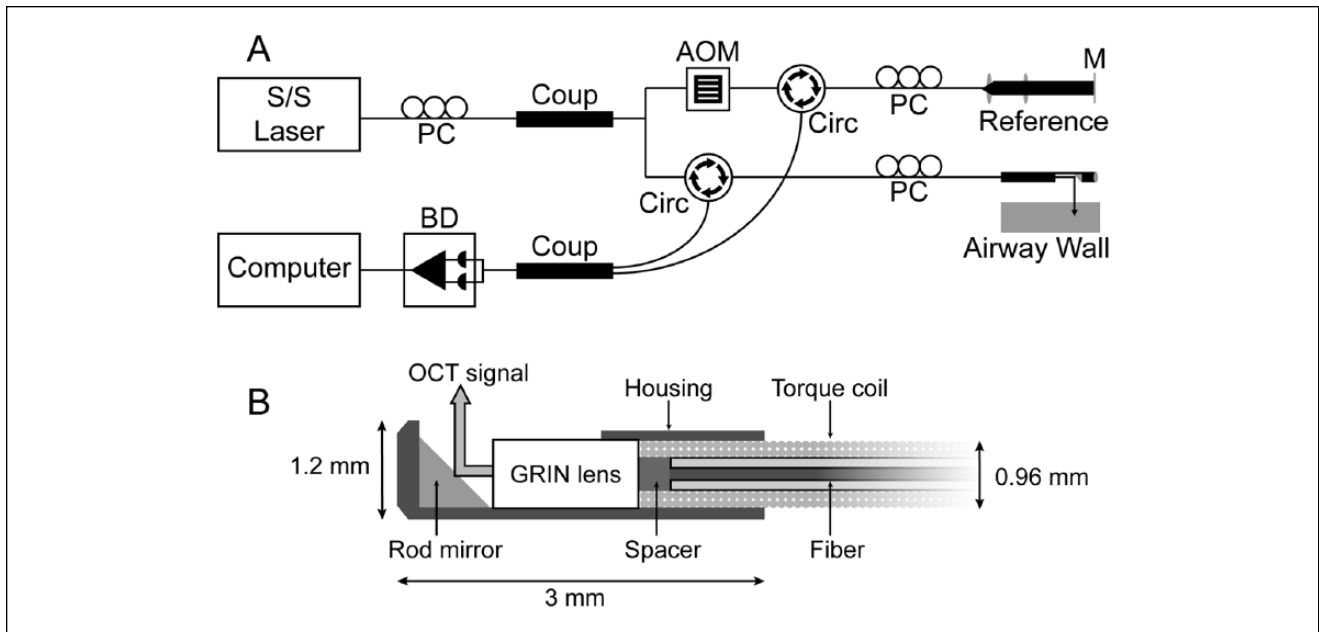


Figure 1. (A) Schematics of long-range optical coherence tomography system and (B) cross-section of the distal cap of a 1.2 mm outer diameter scanning probe.

Abbreviations: AOM, acousto-optic modulator; BD, balance detector; Circ, circulator; Coup, coupler; GRIN, gradient refractive index; M, mirror; PC, polarization controller; S/S, swept source.

Image Analysis

Continuous helical scanning of the airway generated 250 to 300 raw LR-OCT images in Cartesian coordinates. Raw data were converted into polar coordinates to yield anatomically correct, axial images (MATLAB; MathWorks, Natick, Massachusetts, USA). Airway anatomical landmarks were identified based on distinct topographical characteristics and locations of structures such as the vocal folds, cricoid cartilage, and tracheal rings. Between the cranial and caudal limits of the stenotic segment, each consecutive axial LR-OCT frame was measured for anteroposterior (AP) diameter, transverse diameter, and intraluminal cross-sectional area (CSA) using software coded in MATLAB. For each patient, the corresponding postintervention LR-OCT data set was measured over the same segment of airway to yield an equal number of measured images as the pre-intervention data set. Differences between pre-intervention and postintervention measurements were analyzed using a paired *t* test ($\alpha = .05$). The distance between the vocal cords and the proximal limit of stenosis, as well as the cranio-caudal length of the stenotic segment, were also measured in the pre-intervention data sets. Statistical analysis was performed using SYSTAT v13.0 (San Jose, California, USA).

The combined thickness of the mucosa and submucosa, hereafter referred to as the airway wall, was measured in all data sets. Airway wall segmentation and

measurement were performed using a MATLAB-based software; detailed description of this methodology has been reported.²⁵ Previous OCT studies have also validated similar software-based airway tissue measurement by comparative analysis with CT and histology.²⁶⁻²⁸ The LR-OCT data sets were divided into 3 anatomic groups, larynx, subglottis, and trachea, based on anatomical landmarks identified on OCT. In each cross-sectional LR-OCT image frame, the airway wall was segmented by tracing the luminal surface and submucosa-perichondrium interface using a drawing tablet (Intuos 5; Wacom, Vancouver, Washington, USA) and software encoded in MATLAB. Airway wall thickness was automatically calculated for the segmented tissue in each frame and averaged over the subset of frames within each anatomic group. The thickness of the sheath wall was used as a reference measurement, and the refractive indices of light in biological tissue and plastic were taken into account for thickness calculations.²⁵

3-D Airway Models

Detailed methodology of airway model generation has been previously described.²⁵ Semi-automated data post processing included manual segmentation of the luminal surface of the airway in each 2-dimensional axial LR-OCT frame within a data set. Segmented axial images were coalesced into an array and rendered into 3-D airway models (MIMICS; Materialise, Plymouth, Michigan, USA).

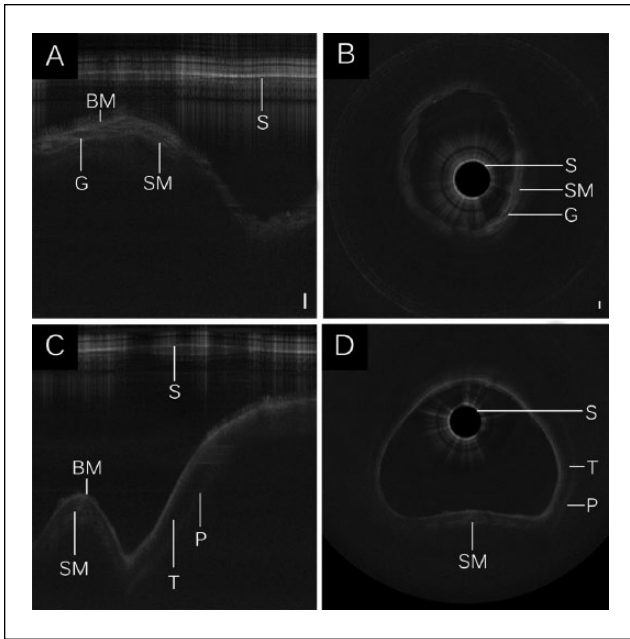


Figure 2. Long-range optical coherence tomography images of the (A-B) subglottis and (C-D) trachea. Select segments of raw LR-OCT frames of the (A) subglottis and (C) trachea are displayed in Cartesian coordinates. Data conversion to polar coordinates depicts (B, D) the airway in an axial representation. Noise bands were removed for image clarity. Bar = 500 μ m. Abbreviations: BM, basement membrane; G, submucosal gland; P, perichondrium; S, sheath; SM, submucosa; T, tracheal cartilage.

Results

The LR-OCT was performed during suspension microlaryngoscopy on 3 adult female subjects (mean age 43 years) before and after endoscopic treatment for SGS. All 3 subjects were imaged without OCT-related adverse events or technical complications. The mean data acquisition time for a single airway scan was 20 seconds.

LR-OCT Image Analysis

As light propagates through biological tissue, some photons are backscattered. The intensity of backscattered signal depends on optical properties of tissue (eg, scattering, anisotropy, and absorption) in the light pathway in both forward and backward directions. In OCT imaging, turbid media are represented as a heterogeneous configuration of grey-scale intensities. When light passes through media with minimal or absent scattering effects, such as glandular lumen or water, signal intensity is weak, and image pixels appear dark. Highly scattering tissues such as dense collagen or cartilage surface reflect more signal and appear as near-white or white pixels. Analogous to the effect of bone or cartilage in ultrasonography, dense tissues often create an optical shadow. All LR-OCT data sets in the present study

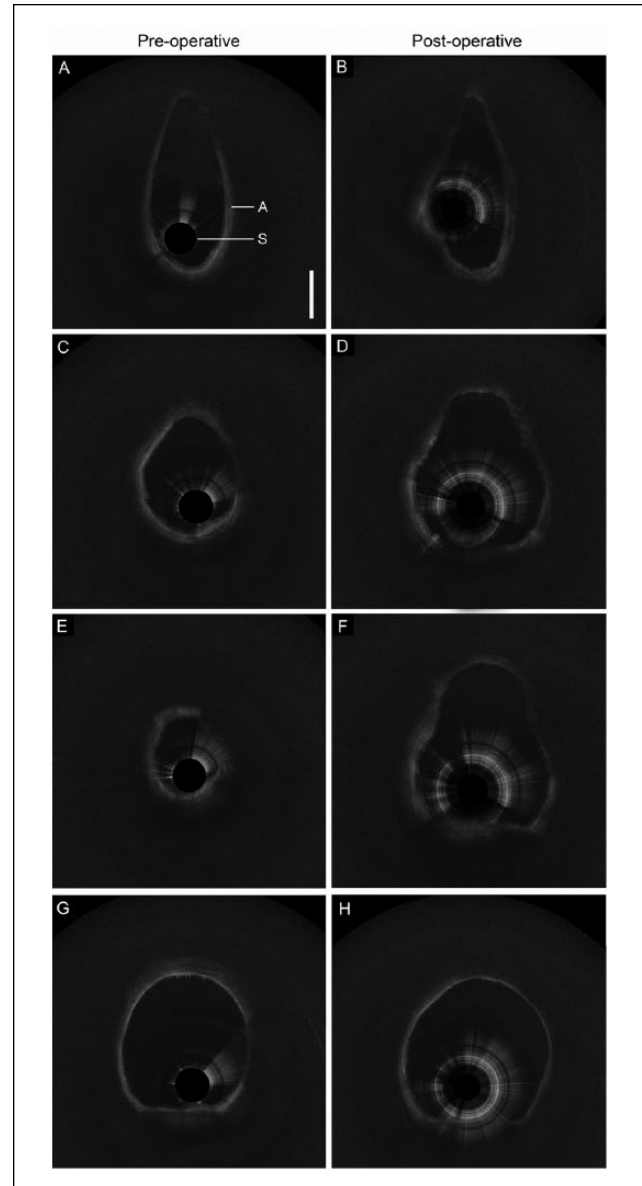


Figure 3. Preoperative and postoperative long-range optical coherence tomography data with select axial frames from the (A-B) larynx, (C-D) proximal subglottis, (E-F) distal subglottis, and (G-H) trachea.

had adequate signal-to-noise ratio and clearly demonstrated anatomical landmarks within the airway. The layered architecture of the airway, including basement membrane, submucosa, and cartilage, were identified (Figure 2). Additional structural features such as the submucosal glands and perichondrium were also identified. Axial LR-OCT images of the larynx (Figure 3 A-B), subglottis (Figure 3 C-F), and trachea (Figure 3 G-H), acquired before and after intervention in subject No. 1, are shown for comparison. Postintervention axial images of the subglottis demonstrate a clear increase in intraluminal CSA.

Table 1. Comparison Between Pre-Intervention and Postintervention Airway Cross-sectional Diameter and Area (Paired *t* test).

	Patient No. 1			Patient No. 2			Patient No. 3					
	N ^a	Preoperative	Postoperative	P Value [†]	N ^a	Preoperative	Postoperative	P Value [†]	N ^a	Preoperative	Postoperative	P Value [†]
AP diameter, mm; mean (SD)	44	13.52 (2.46)	17.95 (1.50)	<.001	77	13.30 (2.14)	15.27 (1.65)	<.001	38	13.95 (4.69)	16.32 (2.05)	.009
Transverse diameter, mm; mean, (SD)	44	9.58 (1.70)	12.74 (1.26)	<.001	77	11.37 (0.63)	15.0 (2.73)	<.001	38	9.47 (2.40)	13.79 (2.17)	<.001
CSA, mm ² ; mean, (SD)	44	106.73 (33.46)	166.81 (27.09)	<.001	77	124 (19.36)	196.48 (42.67)	<.001	38	109.5 (56.93)	179.9 (43.88)	<.001

Abbreviations: AP, anteroposterior; CSA, cross-sectional area; SD, standard deviation.

^aNumber of axial long-range optical coherence tomography image frames (500 μ m separation) measured within the stenotic segment of the airway.

[†]Paired *t* test ($\alpha = .05$).

Table 2. Mean Airway Wall Thickness (μ m) in Pre-Intervention and Postintervention Long-range Optical Coherence Tomography Data Sets.

	Patient No. 1		Patient No. 2		Patient No. 3	
	Pre-Intervention	Postintervention	Pre-Intervention	Postintervention	Pre-Intervention	Postintervention
Larynx, μ m; mean (SD)	676.33 (45.86)	716.23 (97.59)	713.43 (63.33)	684.97 (68.44)	709.34 (51.44)	712.40 (61.43)
Subglottis, μ m; mean (SD)	671.79 (27.32)	687.01 (47.71)	664.79 (35.37)	692.92 (71.98)	684.16 (58.62)	701.94 (66.18)
Trachea, μ m; mean (SD)	597.01 (40.17)	604.77 (29.02)	606.61 (22.79)	580.38 (15.97)	673.45 (25.67)	680.29 (33.24)

Abbreviations: Airway wall, combined thickness of mucosa and submucosa, excluding cartilage; SD, standard deviation.

Statistically significant differences in mean AP diameter ($P < .01$), transverse diameter ($P < .001$), and CSA ($P < .001$) were noted between pre-intervention and postintervention data sets for all 3 patients (Table 1). The measured distance between the vocal cords and the proximal limit of SGS was 14.0 mm in patient No. 1, 13.5 mm in patient No. 2, and 12.5 mm in patient No. 3. The craniocaudal length of the SGS was 7.0 mm in patient No. 1, 27.5 mm in patient No. 2, and 15.0 mm in patient No. 3. Mean airway wall thickness measurements are presented in Table 2. In all 3 patients, an increase in mean subglottic wall thickness was noted following endoscopic intervention. Patient Nos. 1 and 3 also demonstrated increases in mean laryngeal wall thickness following intervention.

3-D Airway Models

Digital airway models were generated from LR-OCT data sets (Figure 4). Postintervention models for all 3 subjects demonstrated an increase in airway patency at the levels of the subglottis and proximal trachea. Video 1 depicts virtual bronchoscopy of the pre-intervention and postintervention airway model for patient No. 1.

Discussion

At present, there are limited options to practically and accurately measure the dimensions of the stenotic airway. Objective, patient-specific data on airway geometry would potentially assist surgeons in making management

decisions, gauging the efficacy of intervention, and quantifying the rate of disease progression. In this study, LR-OCT imaging was performed to practically measure the dimensions of SGS during suspension microlaryngoscopy before and after treatment.

The measurement accuracy of a diagnostic imaging modality is largely determined by its resolution. With micrometer-level resolution, OCT is uniquely capable of providing accurate, intraluminal measurements of SGS. In 2014, Wijesundara et al²³ compared swept-source OCT and calipers (reference standard) to measure the inner dimensions of various cylindrical tubes. Mean CSA measurements using OCT were found to be $1.4\% \pm 1.0\%$ less than caliper-based CSA measurements. In a similar study, Williamson et al¹⁷ measured plastic tubes (diameters 2.6-50.0 mm) using OCT and internal calipers and reported a mean difference in CSA of $-0.1 \pm 5.6 \text{ mm}^2$ ($-0.3\% \pm 3.5\%$) across all tubes.

In the present study, while each patient had a statistically significant increase in airway CSA following intervention, the individual response to treatment was variable. All 3 patients were treated with endoscopic laser lysis and 15 mm balloon dilation. However, the mean postintervention diameters in patient No. 1, patient No. 2, and patient No. 3 were 17.95 mm (Δ CSA + 56.3%), 15.27 mm (Δ CSA + 58.4%), and 16.32 mm (Δ CSA + 64.4%), respectively. These differences suggest that the immediate response to treatment of SGS is dependent on a myriad of patient-specific factors, including the degree of stenosis, depth and maturation of scar tissue, and extent of intervention performed.

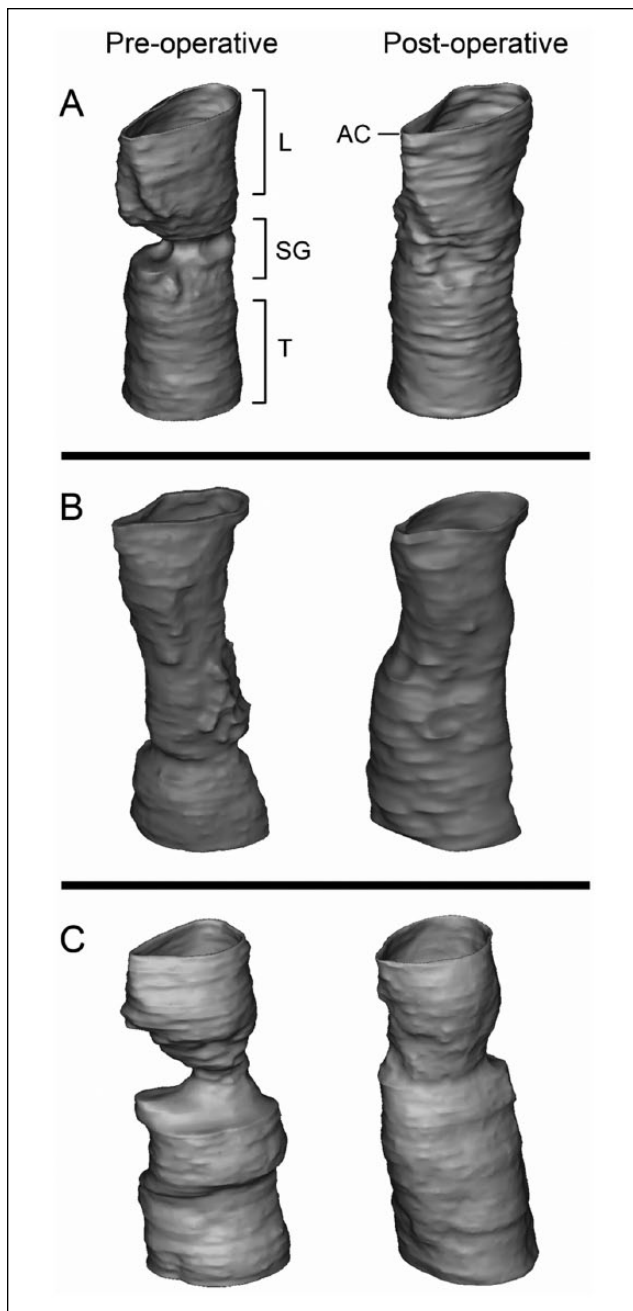


Figure 4. Three-dimensional airway models based on preoperative and postoperative long-range optical coherence tomography data for (A) patient No. 1, (B) patient No. 2, and (C) patient No. 3.

The long-term response to treatment can be further influenced by intraoperative application of topical mitomycin-C²⁹ and each patient's unique biology of wound healing. Without precise measurements of the airway pre-intervention, immediately postdilation and at long-term follow-up, the efficacy of treatment is limited to subjective data and clinical symptoms.

In all 3 patients, an increase in mean subglottic airway wall thickness was noted after intervention. While the low sample size precludes a statistically supported trend or clinical correlation, it is plausible that this finding may be secondary to acute submucosal inflammation and edema following intervention. In a previous study, transendotracheal tube LR-OCT was performed in series of 72 neonates to evaluate the effects of endotracheal intubation on the airway wall.¹⁹ A positive correlation between mean laryngeal and subglottic wall thickness and duration of intubation was noted. The rate of increase in wall thickness was highest in the first 72 hours, correlating with the inflammatory phase of wound healing. The OCT image analysis depicted submucosal glandular dilatation in patients following short-term intubation (≤ 7 days) and, in select cases, dense, high-intensity submucosa suggestive of fibrosis following long-term intubations (8+ days).¹⁹

Advantages of LR-OCT

In this study, airway diameter and CSA measurements were acquired offline, after the surgery was completed. However, the OCT software used in this study allows for real-time generation and storage of data. Hence, airway dimensions can also be measured intraoperatively, immediately after scanning the airway. Real-time airway dimensions may ultimately help surgeons formulate and optimize individualized operative plans. Furthermore, selection of an appropriately sized balloon dilators based on pre-intervention measurements would help reduce resource consumption and increase operative efficiency.

Similar to CT multiplanar reformation, 3-D reconstructions of the airway can be generated in MIMICS and visualized in cross-sectional sagittal and coronal planes. An axis of rotation can also be defined for comprehensive evaluation of the external shell. Additionally, the dimensions of SGS, such as the distance between the vocal folds and the stenotic segment, the cranio-caudal length of SGS, and the spatial distribution of scar tissue, are all additional dimensions that can be measured in MIMICS. These data may further contribute to SGS management decisions, such as localization of scar tissue prior to laser lysis or planning for open surgical intervention. Long-range optical coherence tomography adds to the benefits of the previously described K-wire "measuring stick" by providing cross-sectional imaging and allowing for characterization of subepithelial scar tissue within the airway wall.^{18,19}

Applications and Future Steps

This is not the only application of LR-OCT in airway evaluation. Previous studies describe the safety and efficacy of intraoperative LR-OCT imaging of the pediatric upper airway^{18,21} and bedside LR-OCT imaging of the intubated

neonatal airway¹⁹ to measure airway dimensions. Long-range optical coherence tomography imaging of the pharyngeal airway has also been performed in awake adults^{16,24,30} and children³¹ with the objective to perform dynamic evaluation of the airway in patients with obstructive upper airway disease. Lazarow et al³¹ reported the first series of tandem OCT and flexible nasopharyngoscopy in awake pediatric patients with sleep-disordered breathing. The OCT data were analyzed for structural anatomy, and 3-D volumetric renderings were used to visualize the intraluminal geometry and identify areas of stenosis. Current research efforts include LR-OCT imaging during drug-induced sleep endoscopy studies to dynamically evaluate the upper airway during the full sleep cycle, with the aim to potentially help surgeons localize airway stenosis based on objective data.

The natural extension of the current study is to perform LR-OCT in awake patients to evaluate the subglottis and trachea during office-based transnasal tracheoscopy.^{9,32} Tandem OCT and flexible nasopharyngoscopy has been described previously.^{23,31} Most commercial adult flexible laryngoscopes have working channels between 2.0 mm to 2.2 mm inner diameter. While the sheaths used in this study (2.08 mm outer diameter/OD) are not conducive for easy instrumentation through a working channel, LR-OCT of the airway has been previously described using 0.7 mm diameter probes and sheaths with ≤ 1.37 mm OD.^{18,19,31} These smaller profile probes are optimal for tandem LR-OCT imaging during transnasal tracheoscopy. Accurate measurement of SGS dimensions during outpatient evaluation may further assist surgeons in making management decisions and/or gauging the rate of disease progression. Three-dimensional airway models created from LR-OCT data may ultimately be used to calculate predictive models for airflow resistance using computational fluid dynamics.³³

Limitations

Some limitations to OCT technology and to this study are worth noting. Presently, there are no commercial LR-OCT systems available for diagnostic imaging of the head and neck. The research LR-OCT system (Figure 1A) designed and constructed by this group remains investigational and requires an engineer to operate. As OCT technology evolves, standalone systems for head and neck imaging may be available in the future. While the advancement of LR-OCT systems and more recently, vertical cavity surface-emitting laser (VCSEL)-based OCT systems now permit extended range axial imaging up to 25 mm, the diagnostic value of OCT remains limited by signal penetration depth of approximately 1.5 mm into tissue. Therefore, in highly scarred and stenotic airways, measurement of the full depth of scar tissue may not be feasible.

A challenge associated with upper airway OCT imaging is maintaining consistency with image quality. Variability in

signal strength and image quality is largely secondary to interprobe variability in the distal optical assembly (Figure 1B), which is manually constructed under microscopy. Furthermore, high-speed rotation of probes through a tortuous path causes fine precession of the distal optical assembly, which may result in motion artifact. As the probe recoils within the sheath, friction between the probe coil and inner surface of the sheath may result in further image distortion. Hence, standardization of probe assembly is critical for acquiring consistent, high-quality data. After refinement of our probe fabrication protocol, more recent upper airway OCT studies by our group have data yield up to 71%.¹⁹

Conclusion

Long-range optical coherence tomography is a practical and safe diagnostic imaging technology that can be used to acquire accurate measurements of SGS during suspension microlaryngoscopy. As demonstrated in this study, individual response to the same therapy is variable, underscoring the value in measuring pre-intervention SGS dimensions. Lastly, LR-OCT allows the surgeon to measure post-dilation changes in the airway and quantify the immediate response to therapy.

Authors' Note

Presented at the 93rd annual meeting of the American Bronchoesophagological Association. Orlando, Florida. April 10, 2013. Authors G.K.S. and A.C. are co-first authors.

Acknowledgments

We would like to thank Kathryn Osann, PhD, for her assistance with statistical analysis.

Declaration of Conflicting Interests

The author(s) declared no potential conflicts of interest with respect to the research, authorship, and/or publication of this article.

Funding

The author(s) disclosed receipt of the following financial support for the research, authorship, and/or publication of this article: Air Force Office of Scientific Research (FA9550-04-1-0101), National Institutes of Health (NIH/NHLBI/NIDCD 1-R01-HL103764-01, NIH/NHLBI 1-R01-HL105215-01), Tobacco-related disease research program (TRDRP 19KT-0034).

References

1. Patel H, Goldenberg D, McGinn J. Surgical management of upper airway stenosis. In: Flint P, ed. *Cummings Otolaryngology: Head and Neck Surgery*. Vol 3, 6th ed. Philadelphia, PA: Saunders; 2015:982-992.
2. Zalzal G, Cotton R. Glottic and subglottic stenosis. In: Lesperance M, ed. *Cummings Otolaryngology: Head and Neck Surgery*. Vol 3, 6th ed. Philadelphia, PA: Saunders; 2015:3158-3170.

3. Dumoulin E, Stather DR, Gelfand G, Maranda B, Maceachern P, Tremblay A. Idiopathic subglottic stenosis: a familial predisposition. *Ann Thorac Surg*. 2013;95(3):1084-1086.
4. Myer CM, 3rd, O'Connor DM, Cotton RT. Proposed grading system for subglottic stenosis based on endotracheal tube sizes. *Ann Otol Rhinol Laryngol*. 1994;103(4 Pt 1):319-323.
5. Jewett BS, Cook RD, Johnson KL, et al. Subglottic stenosis: correlation between computed tomography and bronchoscopy. *Ann Otol Rhinol Laryngol*. 1999;108(9):837-841.
6. Brenner DJ, Hall EJ. Computed tomography—an increasing source of radiation exposure. *N Engl J Med*. 2007;357(22):2277-2284.
7. Lewis TA, Tzeng YS, McKinstry EL, et al. Quantification of airway diameters and 3D airway tree rendering from dynamic hyperpolarized 3He magnetic resonance imaging. *Magn Reson Med*. 2005;53(2):474-478.
8. Sharma GK, Foulad A, Verma SP. A novel device for measurement of subglottic stenosis in 3 dimensions during suspension laryngoscopy. *JAMA Otolaryngol Head Neck Surg*. 2015;141(4):377-381.
9. Verma SP, Smith ME, Dailey SH. Transnasal tracheoscopy. *Laryngoscope*. 2012;122(6):1326-1330.
10. Nouraei SA, McPartlin DW, Nouraei SM, et al. Objective sizing of upper airway stenosis: a quantitative endoscopic approach. *Laryngoscope*. 2006;116(1):12-17.
11. Kanamori A, Nakamura M, Matsui N, et al. Optical coherence tomography detects characteristic retinal nerve fiber layer thickness corresponding to band atrophy of the optic discs. *Ophthalmology*. 2004;111(12):2278-2283.
12. Sandali O, El Sanharawi M, Temstet C, et al. Fourier-domain optical coherence tomography imaging in keratoconus: a corneal structural classification. *Ophthalmology*. 2013;120(12):2403-2412.
13. Jang IK, Bouma BE, Kang DH, et al. Visualization of coronary atherosclerotic plaques in patients using optical coherence tomography: comparison with intravascular ultrasound. *J Am Coll Cardiol*. 2002;39(4):604-609.
14. Yabushita H, Bouma BE, Houser SL, et al. Characterization of human atherosclerosis by optical coherence tomography. *Circulation*. 2002;106(13):1640-1645.
15. Armstrong J, Leigh M, Walton I, et al. In vivo size and shape measurement of the human upper airway using endoscopic longrange optical coherence tomography. *Opt Express*. 2003;11(15):1817-1826.
16. Armstrong JJ, Leigh MS, Sampson DD, Walsh JH, Hillman DR, Eastwood PR. Quantitative upper airway imaging with anatomic optical coherence tomography. *Am J Respir Crit Care Med*. 2006;173(2):226-233.
17. Williamson JP, Armstrong JJ, McLaughlin RA, et al. Measuring airway dimensions during bronchoscopy using anatomical optical coherence tomography. *Eur Respir J*. 2010;35(1):34-41.
18. Volgger V, Sharma GK, Jing JC, et al. Long-range Fourier domain optical coherence tomography of the pediatric subglottis. *Int J Pediatr Otorhinolaryngol*. 2015;79(2):119-126.
19. Sharma GK, Ahuja GS, Wiedmann M, et al. Long range optical coherence tomography of the neonatal upper airway for early diagnosis of intubation-related subglottic injury. *Am J Respir Crit Care Med*. 2015;192(12):1504-1513.
20. Huang D, Swanson EA, Lin CP, et al. Optical coherence tomography. *Science*. 1991;254(5035):1178-1181.
21. Lazarow FB, Ahuja GS, Chin Loy A, et al. Intraoperative long range optical coherence tomography as a novel method of imaging the pediatric upper airway before and after adenotonsillectomy. *Int J Pediatr Otorhinolaryngol*. 2015;79(1):63-70.
22. Williamson JP, McLaughlin RA, Phillips MJ, et al. Feasibility of applying real-time optical imaging during bronchoscopic interventions for central airway obstruction. *J Bronchology Interv Pulmonol*. 2010;17(4):307-316.
23. Wijesundara K, Zdanski C, Kimbell J, Price H, Ifimia N, Oldenburg AL. Quantitative upper airway endoscopy with swept-source anatomical optical coherence tomography. *Biomed Opt Express*. 2014;5(3):788-799.
24. Jing J, Zhang J, Loy AC, Wong BJ, Chen Z. High-speed upper-airway imaging using full-range optical coherence tomography. *J Biomed Opt*. 2012;17(11):110507.
25. Su E, Sharma G, Chen J, et al. Analysis and digital 3D modelings of long-range Fourier-domain optical coherence tomography images of the pediatric subglottis. *Proceedings of SPIE*, 2014:8926.
26. Coxson HO, Quiney B, Sin DD, et al. Airway wall thickness assessed using computed tomography and optical coherence tomography. *Am J Respir Crit Care Med*. 2008;177(11):1201-1206.
27. Lee AM, Kirby M, Ohtani K, et al. Validation of airway wall measurements by optical coherence tomography in porcine airways. *PLoS One*. 2014;9(6):e100145.
28. Kaiser ML, Rubinstein M, Vokes DE, et al. Laryngeal epithelial thickness: a comparison between optical coherence tomography and histology. *Clin Otolaryngol*. 2009;34(5):460-466.
29. Smith ME, Elstad M. Mitomycin C and the endoscopic treatment of laryngotracheal stenosis: are two applications better than one? *Laryngoscope*. 2009;119(2):272-283.
30. Walsh JH, Leigh MS, Paduch A, et al. Evaluation of pharyngeal shape and size using anatomical optical coherence tomography in individuals with and without obstructive sleep apnoea. *J Sleep Res*. 2008;17(2):230-238.
31. Lazarow F, Ahuja G, Sharma G, et al. First use of long-range optical coherence tomography to image airway structure in awake children. *Otolaryngol Head Neck Surg*. 2014;151(1):133.
32. Sharma GK, Verma SP. Is nebulized lidocaine adequate topical anesthesia for diagnostic transnasal tracheoscopy? *Ann Otol Rhinol Laryngol*. 2015;124(7):545-549.
33. Wang Y, Elghobashi S. On locating the obstruction in the upper airway via numerical simulation. *Respir Physiol Neurobiol*. 2014;193:1-10.